Conformational Space

DOI: 10.1002/anie.201406145

Exploration of Conformational Spaces of High-Mannose-Type Oligosaccharides by an NMR-Validated Simulation**

*Takumi Yamaguchi, Yoshitake Sakae, Ying Zhang, Sayoko Yamamoto, Yuko Okamoto, and Koichi Kato**

Abstract: *Exploration of the conformational spaces of flexible biomacromolecules is essential for quantitatively understanding the energetics of their molecular recognition processes. We employed stable isotope- and lanthanide-assisted NMR approaches in conjunction with replica-exchange molecular dynamics (REMD) simulations to obtain atomic descriptions of the conformational dynamics of high-mannose-type oligosaccharides, which harbor intracellular glycoprotein-fate determinants in their triantennary structures. The experimentally validated REMD simulation provided quantitative views of the dynamic conformational ensembles of the complicated, branched oligosaccharides, and indicated significant expansion of the conformational space upon removal of a terminal mannose residue during the functional glycan-processing pathway.*

Conformational dynamics are essential properties of biomacromolecules that are involved in molecular recognition events in living systems.[1] The motional freedom of three-dimensional structures can endow them with adaptability to various interaction partners, occasionally in promiscuous fashions as exemplified by intrinsically disordered proteins. Based primarily on crystallographic analyses, structural data have been accumulated for biomacromolecules in complexes with their binding partners. However, for quantitative understanding of their binding mechanisms and energetics, the conformational spaces occupied by these flexible biomolecules in their free states should be explored by considering changes in the conformational entropy and preexisting conformers selected upon binding.

Oligosaccharides are typical biomacromolecules with numerous degrees of motional freedom and with conformational adaptability to their binding proteins, which are collectively termed lectins.[2] The unique features of this class of flexible biomacromolecules are their branching structures, which often contain homologous antennae composed of identical residues. The conformational spaces of oligosaccharides have been explored by using computational techniques such as molecular mechanics and molecular dynamics (MD) simulations,[3,4] including those based on a generalized-ensemble algorithm.[5] Moreover, NMR spectroscopy has been employed for experimental characterization of the dynamic conformations of oligosaccharides, typically through inspection of scalar couplings and nuclear Overhauser effect data;[6,7] however, these data provide only limited local conformational restraints and are often difficult to fully analyze because of the poor spectral resolution that results from small variations in functional groups.

The most promising solution to this problem is the use of paramagnetic effects, which provide long-distance information in the structural characterization of biomolecules.[8] Recently, paramagnetism-assisted NMR techniques were developed to characterize the overall conformations of oligosaccharides in solution.[9] In this method, paramagnetic effects such as pseudocontact shift (PCS)[10] and relaxation enhancement[11] are used as sources of atomic long-distance information. We have demonstrated that long-timescale MD simulations validated by experimentally observed PCS data allow for adequate exploration of the conformational spaces of small oligosaccharides, such as the GM3 trisaccharide and GM2 tetrasaccharide.[10c,d] However, it is not clear whether this method is applicable to larger, highly branched sugar chains with rough energy landscapes of very high dimensions.

To address this issue, we herein report the atomic descriptions of the conformational dynamics in triantennary high-mannose-type oligosaccharides based on a hybrid approach that combines NMR spectroscopy and MD simulation. This class of oligosaccharides plays an important role in intracellular glycoprotein-fate determination by interacting with a series of lectins as guides for folding, secretory, and

[*] Dr. T. Yamaguchi, Dr. Y. Zhang, S. Yamamoto, Prof. K. Kato
Institute for Molecular Science and
Okazaki Institute for Integrative Bioscience
5-1 Higashiyama, Myodaiji, Okazaki, 444-8787 (Japan)
and
Graduate School of Pharmaceutical Sciences
Nagoya City University
3-1 Tanabe-dori, Mizuho-ku, Nagoya 467-8603 (Japan)
E-mail: kkatonmr@ims.ac.jp
Dr. T. Yamaguchi, Dr. Y. Zhang, Prof. K. Kato
School of Physical Sciences
The Graduate University for Advanced Studies
5-1 Higashiyama, Myodaiji, Okazaki, 444-8787 (Japan)
Dr. Y. Sakae, Prof. Y. Okamoto
School of Sciences, Nagoya University
Furo-cho, Chikusa-ku, Nagoya, 464-8602 (Japan)

[**] We thank Dr. Yasunori Chiba and Dr. Toshihiko Kitajima (The National Institute of Advanced Industrial Science and Technology) for providing the engineered yeast cells, Dr. Takahisa Ikegami (Osaka University) for his help with the NMR measurements, and Yukiko Isono (IMS) for her help in the preparation of the oligosaccharides. The NMR analyses in this study were performed, in part, under the Cooperative Research Program of the Institute for Protein Research, Osaka University. This work was partly supported by the Nanotechnology Platform Program of MEXT (Japan), MEXT/JSPS Grants in Aid for Scientific Research (25102008, 25102009, 24249002, 26560451and 24750170), and the Okazaki ORION project.

Supporting information for this article is available on the WWW under http://dx.doi.org/10.1002/anie.201406145.

degradation processes.[12] In this quality control system, a newly synthesized protein is tagged with the high-mannose-type oligosaccharide, which originally contains nine mannose residues and harbors distinct fate determinants in its triantennary structure.[13] Subsequent enzymatic trimming of their outer mannose residues is coupled with exposure of the fate determinant for recognition by the intracellular lectins.

In this study, we used a triantennary undecasaccharide containing nine mannose residues, namely, Manα1-2Manα1-6(Manα1-2Manα1-3)Manα1-6(Manα1-2Manα1-2Manα1-3)-Manβ1-4GlcNAcβ1-4GlcNAc (M9) and its derivative (M8B), which lacks the nonreducing-terminal mannose residue (D2) at the central branch (termed the D2 branch; Figure 1). The former is enzymatically converted into the latter in the endoplasmic reticulum, which is considered to be a key step for triggering glycoprotein degradation.[14]

To prepare sufficient quantities of homogeneous M9 and M8B with ^{13}C labeling, we utilized genetically engineered yeast strains in which genes responsible for processing high-mannose-type oligosaccharides are knocked out.[15] The yeast cells were cultivated in a medium containing uniformly ^{13}C-labeled glucose as a carbon source, which gave rise to fully ^{13}C-labeled M9 and M8B. An ethylenediaminetetraacetate (EDTA) derivative designed to serve as a lanthanide chelator[10a] was covalently attached to the reducing terminus of the isolated M9 and M8B oligosaccharides (Figure 1) by selective amination and subsequent acylation reactions without any protection/deprotection of the sugar moiety.

A paramagnetic lanthanide ion, such as Tm^{3+}, was added to a solution of these modified oligosaccharides in D_2O to form stable 1:1 complexes. We confirmed the appearance of a new set of NMR signals with concomitant disappearance of the original signals as a result of the lanthanide-induced PCSs. The ^{13}C labeling of the oligosaccharides enabled us to perform sequential assignments of the observed HSQC signals by HSQC-TOCSY and ^{13}C-edited NOESY experiments, which were facilitated by PCS-induced chemical shift dispersion as a bonus effect. The PCS values were measured as differences between the chemical shifts of each CH group of the oligosaccharides attached to the paramagnetic ion and those observed with the diamagnetic La^{3+} ion (Figure 2). The

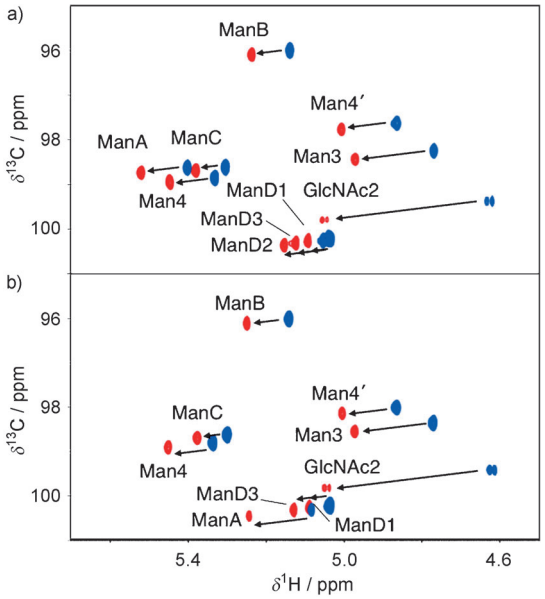

Figure 2. ^{1}H-^{13}C HSQC spectra of the anomeric region of the a) M9 undecasaccharide and b) M8B decasaccharide tagged with Tm^{3+} (red) and La^{3+} (blue). Chemical shift differences induced by PCS are indicated by arrows.

signals attributable to the anomeric CH groups of the terminal mannose residues D1 (D2) and D3 were overlapped under diamagnetic conditions in both M9 and M8B, thus indicating that the local chemical environments surrounding these terminal α-1,2-mannose residues are very similar. However, these signals provided different chemical shifts on addition of Tm^{3+} ions because of different PCSs reflecting the

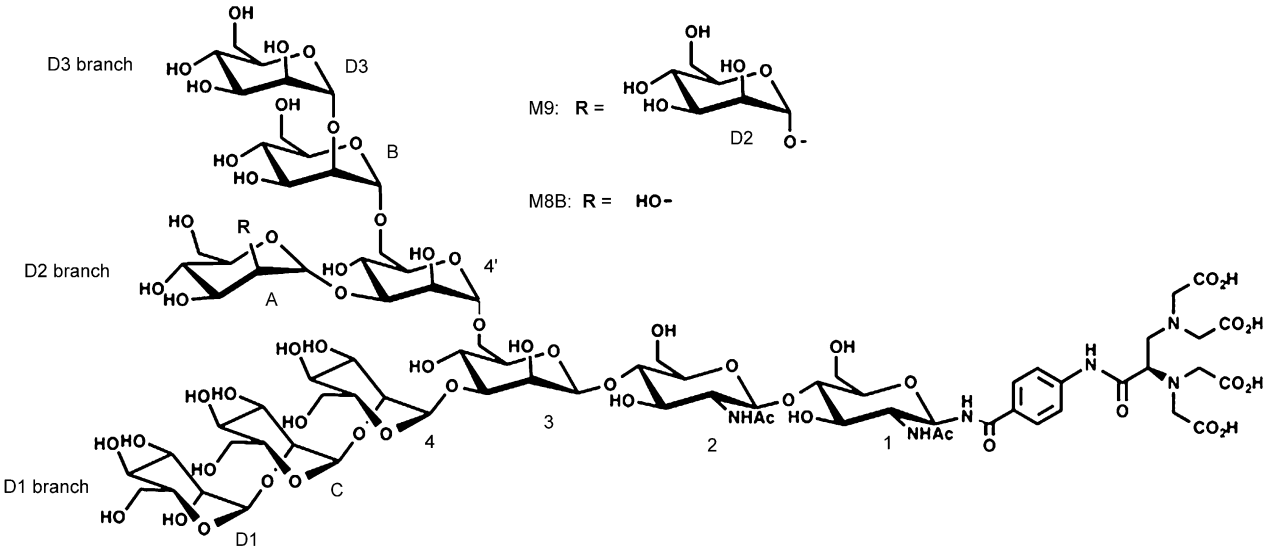

Figure 1. Representation of the high-mannose-type oligosaccharides M9 and M8B modified with the lanthanide ion binding tag.

distinct spatial arrangements of the nonreducing-terminal mannose residues with respect to the lanthanide ion attached to the reducing terminus. Moreover, the ManA and ManB residues exhibited significantly different PCS values between M8B and M9, in contrast to the residues in the D1 branch, which showed marginal differences in the PCS (see Table S1 in the Supporting Information). These data imply the impact of trimming the D2 residue on the conformations of the D2 and D3 branches, which is qualitatively consistent with previous NMR studies on M8B and M9 based on NOE and scalar coupling data.[7,15b]

To interpret the observed PCS data in terms of the dynamic conformational ensemble of oligosaccharides, we performed MD simulations on M8B and M9 in explicit water. From the MD trajectories, 24000 conformers were extracted to develop ensemble models representing possible conformational spaces of the oligosaccharides. According to previously developed methods,[10c] the PCS values of the oligosaccharides with Tm^{3+} ions were back-calculated from these ensemble models (see the Supporting Information), and they were compared with experimentally observed values. In contrast to the situations of smaller tri- and tetrasaccharides, the ensemble models derived from MD simulations over a total of 240 ns could not reproduce the experimental PCS values in either M9 or M8B, most probably because of the multiple-minima problem (see Figure S1 in the Supporting Information). Even with 64 simulations of 48 ns each (a total simulation time of 3.072 μs), the MD-derived ensemble models provided only compromised Q values (as criteria of agreement between experimental and calculated values) of 0.16 and 0.15 for M9 and M8B, respectively (Figure 3a,b).

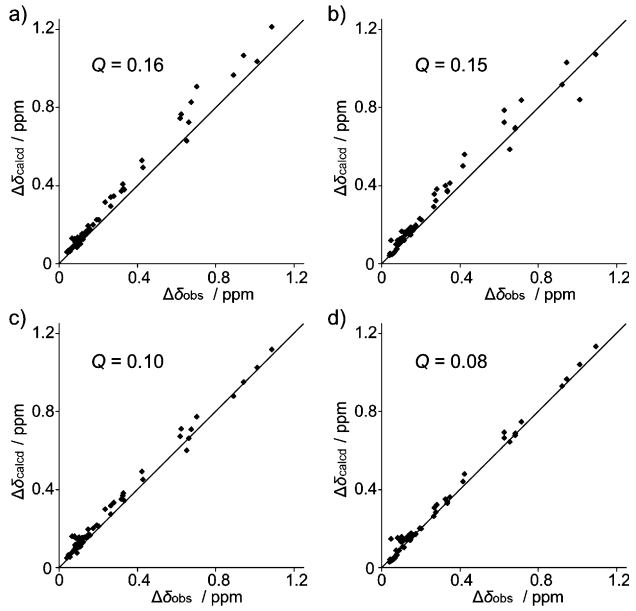

Figure 3. Correlations between experimentally observed PCS values with Tm^{3+} and back-calculated PCS data for M9 (a,c) and for M8B (b,d). The PCS values were back-calculated from the conventional MD-derived (a,b) and the REMD-derived (c,d) ensemble models. Experimentally obtained PCS data for 35 and 33 CH groups from all the residues in M9 and M8B, respectively, were employed.

Thus, to overcome this issue, we employed replica-exchange MD (REMD) simulations[5,16] with the GLYCAM 06 force field[17] in which parallel replicas were run at different temperatures and the coordinates of the replicas were exchanged during the calculation for effective exploration of the high-dimensional rough energy landscapes. To compare with the results from conventional MD simulations, we used 64 replicas, each of which was simulated for 48 ns, and extracted 24000 conformers from each combined trajectory to develop ensemble models. The PCS values back-calculated from the REMD-derived ensemble models were in good agreement with the experimental values: $Q = 0.10$ for M9 and 0.08 for M8B (Figure 3c,d). These results demonstrate the utility of the REMD method for exploring high-dimensional conformational spaces occupied by flexible and branched high-mannose-type oligosaccharides. Similarly, lower Q values were also obtained using REMD simulations with PCS data observed with the lanthanide probes Er^{3+} and Ho^{3+} compared to conventional MD simulations (see Figures S2 and S3 in the Supporting Information).

The experimentally validated REMD data allow us to compare the conformational spaces of the M8B and M9 oligosaccharides. The distribution of distances between the anomeric protons of the reducing-terminal residue (GlcNAc1) and that of each mannose residue was computed from the 24000 conformers extracted from the REMD-derived conformational ensembles (Figure 4). The results clearly demonstrate that, in both M8B and M9, the D2 and D3 branches assume fold-back conformations, in which the outer mannose residues are in spatial proximity to the reducing terminus. Intriguingly, because of the absence of ManD2, the ManA residue, which is located at the nonreducing terminus on the D2 branch in M8B, could more readily obtain access to the reducing terminus in M8B than in M9 (see Figure S4 in the Supporting Information). Note that 5% of the M8B conformers exhibit a ManA–GlcNAc1 distance of < 8 Å, and such conformers occupy < 1% of all the possible conformers in M9 to avoid steric hindrance between ManD2 and the reducing-terminal residues. Moreover, the fold-back conformers of the D3 branch (composed of the ManD3 and ManB residues) are highly populated in M8B compared with those in M9. Hence, the terminal ManD2 residue sterically hinders the fold-back conformations of the D2 and D3 branches and thereby restricts conformational freedom in M9. Thus, the NMR-validated REMD data indicate that outer mannose trimming not only exposes the embedded glycotopes but also expands the conformational space of the remaining parts (even for other branches) of triantennary oligosaccharides.

In contrast, such fold-back conformers were rarely observed during conventional MD simulations, in which spatial arrangements of the D2 and D3 branches of M8B and M9 significantly differ from those derived from the REMD simulations (see Figures S5 and S6 in the Supporting Information). For example, the conventional MD results showed that only 2% of the M8B conformers exhibited a ManA–GlcNAc1 distance of < 8 Å. These data demonstrated that the PCS-based NMR approach is useful for validating the MD-derived conformational spaces of the

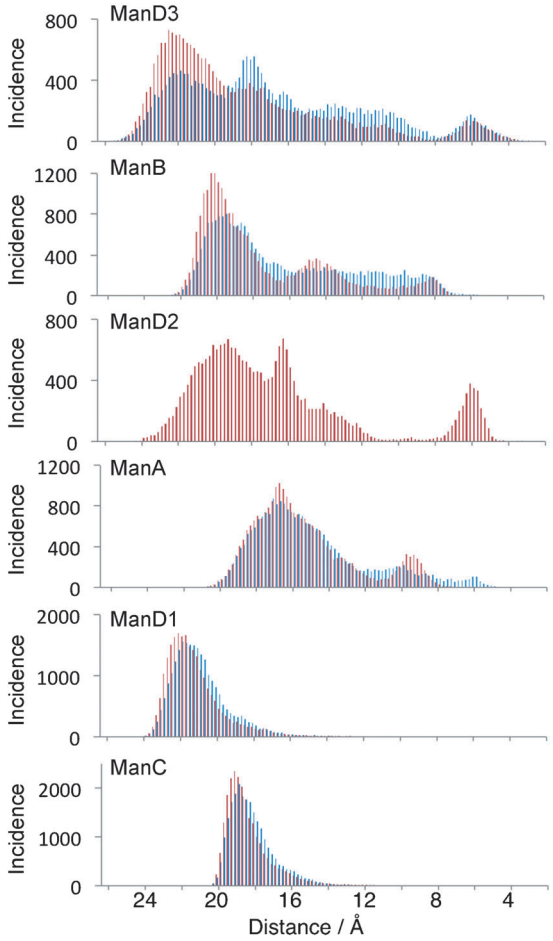

Figure 4. Histograms of the distances between the anomeric protons of the reducing-terminal GlcNAc1 residue and that of each outer mannose residue of M9 (red) and M8B (blue) obtained from the REMD simulations.

highly branched oligosaccharides with quantitative and highly sensitive evaluation of the possible contributions of their minor conformational species.

In summary, we successfully explored the conformational spaces of the high-mannose-type oligosaccharides M9 and M8B in solution by a stable isotope- and lanthanide-assisted NMR spectroscopic approach in conjunction with REMD simulations. Although the overall structural features of these oligosaccharides in the present study are qualitatively consistent with those described in previous reports,[4,7,15b] our results provide quantitative views of the dynamic conformational ensembles of complicated, branched oligosaccharides, which are essential toward understanding the energy landscapes of this class of flexible biomacromolecules.

Received: June 12, 2014
Published online: September 1, 2014

Keywords: lanthanides · molecular dynamics · NMR spectroscopy · oligosaccharides · paramagnetic effects

[1] a) D. D. Boehr, R. Nussinov, P. E. Wright, *Nat. Chem. Biol.* **2009**, *5*, 789–796; b) T. Mittag, L. E. Kay, J. D. Forman-Kay, *J. Mol. Recognit.* **2010**, *23*, 105–116; c) V. N. Uversky, A. K. Dunker, *Biochim. Biophys. Acta Proteins Proteomics* **2010**, *1804*, 1231–1264.
[2] a) H. J. Gabius, S. André, J. Jiménez-Barbero, A. Romero, D. Solís, *Trends Biochem. Sci.* **2011**, *36*, 298–313; b) Y. Kamiya, M. Yagi-Utsumi, H. Yagi, K. Kato, *Curr. Pharm. Des.* **2011**, *17*, 1672–1684.
[3] a) G. A. Jeffrey, R. Taylor, *J. Comput. Chem.* **1980**, *1*, 99–109; b) E. Fadda, R. J. Woods, *Drug Discovery Today* **2010**, *15*, 596–609.
[4] a) R. J. Woods, A. Pathiaseril, M. R. Wormald, C. J. Edge, R. A. Dwek, *Eur. J. Biochem.* **1998**, *258*, 372–386; b) P. V. Balaji, P. K. Qasba, V. S. Rao, *Glycobiology* **1994**, *4*, 497–515.
[5] S. Re, W. Nishima, N. Miyashita, Y. Sugita, *Biophys. Rev.* **2012**, *4*, 179–187.
[6] a) T. Peters, B. M. Pinto, *Curr. Opin. Struct. Biol.* **1996**, *6*, 710–720; b) M. R. Wormald, A. J. Petrescu, Y. L. Pao, A. Glithero, T. Elliott, R. A. Dwek, *Chem. Rev.* **2002**, *102*, 371–386; c) H. Zhao, Q. Pan, W. Zhang, I. Carmichael, A. S. Serianni, *J. Org. Chem.* **2007**, *72*, 7071–7082; d) S. Ilin, C. Bosques, C. Turner, H. Schwalbe, *Angew. Chem.* **2003**, *115*, 1432–1435; *Angew. Chem. Int. Ed.* **2003**, *42*, 1394–1397.
[7] a) S. W. Homans, A. Pastore, R. A. Dwek, T. W. Rademacher, *Biochemistry* **1987**, *26*, 6649–6655; b) E. W. Wooten, R. Bazzo, C. J. Edge, S. Zamze, R. A. Dwek, T. W. Rademacher, *Eur. Biophys. J.* **1990**, *18*, 139–148; c) D. F. Wyss, J. S. Choi, J. Li, M. H. Knoppers, K. J. Willis, A. R. Arulanandam, A. Smolyar, E. L. Reinherz, G. Wagner, *Science* **1995**, *269*, 1273–1278.
[8] a) F. Rodriguez-Castañeda, P. Haberz, A. Leonov, C. Griesinger, *Magn. Reson. Chem.* **2006**, *44*, S10–S16; b) I. Bertini, C. Luchinat, G. Parigi, R. Pierattelli, *Dalton Trans.* **2008**, 3782–3790; c) G. Otting, *Annu. Rev. Biophys.* **2010**, *39*, 387–405.
[9] Y. Zhang, T. Yamaguchi, K. Kato, *Chem. Lett.* **2013**, *42*, 1455–1462.
[10] a) S. Yamamoto, T. Yamaguchi, M. Erdélyi, C. Griesinger, K. Kato, *Chem. Eur. J.* **2011**, *17*, 9280–9282; b) M. Erdélyi, E. d'Auvergne, A. Navarro-Vázquez, A. Leonov, C. Griesinger, *Chem. Eur. J.* **2011**, *17*, 9368–9376; c) S. Yamamoto, Y. Zhang, T. Yamaguchi, T. Kameda, K. Kato, *Chem. Commun.* **2012**, *48*, 4752–4754; d) Y. Zhang, S. Yamamoto, T. Yamaguchi, K. Kato, *Molecules* **2012**, *17*, 6658–6671; e) A. Canales, A. Mallagaray, J. Pérez-Castells, I. Boos, C. Unverzagt, S. André, H.-J. Gabius, F. J. Cañada, J. Jiménez-Barbero, *Angew. Chem.* **2013**, *125*, 14034–14038; *Angew. Chem. Int. Ed.* **2013**, *52*, 13789–13793.
[11] a) M. L. DeMarco, R. J. Woods, J. H. Prestegard, F. Tian, *J. Am. Chem. Soc.* **2010**, *132*, 1334–1338; b) T. Yamaguchi, Y. Kamiya, Y.-M. Choo, S. Yamamoto, K. Kato, *Chem. Lett.* **2013**, *42*, 544–546.
[12] a) K. Kato, Y. Kamiya, *Glycobiology* **2007**, *17*, 1031–1044; b) M. Aebi, R. Bernasconi, S. Clerc, M. Molinari, *Trends Biochem. Sci.* **2010**, *35*, 6962–6971.
[13] Y. Kamiya, T. Satoh, K. Kato, *Biochim. Biophys. Acta Gen. Subj.* **2012**, *1820*, 1327–1337.
[14] a) M. Molinari, *Nat. Chem. Biol.* **2007**, *3*, 313–320; b) N. Hosokawa, Y. Kamiya, K. Kato, *Glycobiology* **2010**, *20*, 651–660.
[15] a) Y. Kamiya, S. Yamamoto, Y. Chiba, Y. Jigami, K. Kato, *J. Biomol. NMR* **2011**, *50*, 397–401; b) Y. Kamiya, K. Yanagi, T. Kitajima, T. Yamaguchi, Y. Chiba, K. Kato, *Biomolecules* **2013**, *3*, 108–123.
[16] Y. Sugita, Y. Okamoto, *Chem. Phys. Lett.* **1999**, *314*, 141–151.
[17] K. N. Kirschner, A. B. Yongye, S. M. Tschampel, J. Gonzalez-Outeirino, C. R. Daniels, B. L. Foley, R. J. Woods, *J. Comput. Chem.* **2008**, *29*, 622–655.

